ChemPubSoc Europe

DOI: 10.1002/chem.201901315

CHEMISTRY A European Journal Full Paper

Molecular Rotors

Enhancing the Viscosity-Sensitive Range of a BODIPY Molecular Rotor by Two Orders of Magnitude**

Stepas Toliautas,[b] Jelena Dodonova,[c] Audrius Žvirblis,[a] Ignas Čiplys,[a] Artūras Polita,[a] Andrius Devižis,[a] Sigitas Tumkevičius,[c] Juozas Šulskus,[b] and Aurimas Vyšniauskas*[a]

Abstract: Molecular rotors are a class of fluorophores that enable convenient imaging of viscosity inside microscopic samples such as lipid vesicles or live cells. Currently, rotor compounds containing a boron-dipyrromethene (BODIPY) group are among the most promising viscosity probes. In this work, it is reported that by adding heavy-electron-withdrawing $-NO_2$ groups, the viscosity-sensitive range of a BODIPY probe is drastically expanded from 5–1500 cP to 0.5–50 000 cP. The improved range makes it, to our knowledge, the first hydrophobic molecular rotor applicable not only at moderate viscosities but also for viscosity measurements in highly viscous samples. Furthermore, the photophysical mechanism of the BODIPY molecular rotors under study has been determined by performing quantum chemical calculations and transient absorption experiments. This mechanism demonstrates how BODIPY molecular rotors work in general, why the $-NO_2$ group causes such an improvement, and why BODIPY molecular rotors suffer from undesirable sensitivity to temperature. Overall, besides reporting a viscosity probe with remarkable properties, the results obtained expand the general understanding of molecular rotors and show a way to use the knowledge of their molecular action mechanism for augmenting their viscosity-sensing properties.

Introduction

Viscosity is quite an important property when microscopic objects such as aerosols or live cells are considered. It determines the rates of diffusion and reactions within the sample as well as its physical properties. However, it is challenging to measure viscosity in such samples because traditional methods are not suitable for microscopic objects. Fortunately, relatively fast and convenient measurements of viscosity can be achieved with an emerging class of fluorescent compounds—molecular rotors.[1,2] Previously, they have been used for viscosity sensing in polymers,[3,4] polymersomes,[5] aerosols,[6–8] model lipid bilayers,[9,10] protein aggregates,[11] and live cells.[12–15] Within cells, viscosity measurements have been performed in mitochondria,[16,17] lysosomes,[18] an endoplasmic reticulum,[19] and a plasma membrane.[20,21] Their main advantage over other methods used for viscosity measurements, such as fluorescence correlation spectroscopy (FCS),[22] fluorescence recovery after photobleaching (FRAP),[23] and single particle tracking (SPT),[24] is the ability to produce spatially resolved viscosity maps of the sample instead of single-point measurements.

Molecular rotors sense viscosity by intramolecular rotation upon excitation.[1] At first, the molecule resides in a fluorescent state. When the rotation occurs, the molecule leaves the fluorescent state and eventually relaxes back to the ground state by a non-radiative transition. In a low viscosity environment, the intramolecular rotation is fast, which leads to a quick deactivation from the fluorescent state, weak fluorescence, short fluorescence lifetime, and vice versa. As the fluorescence intensity depends on the local concentration of the fluorophore and the experimental setup, the fluorescence lifetime is the preferred parameter for assessing viscosity.

BODIPY-C_{12} (Figure 1) and its variations containing other ether groups as substituents are arguably the most widely

[a] A. Žvirblis, I. Čiplys, A. Polita, Dr. A. Devižis, Dr. A. Vyšniauskas
Center of Physical Sciences and Technology
Saulėtekio av. 3, Vilnius, 10257 (Lithuania)
E-mail: aurimas.vysniauskas@ftmc.lt

[b] Dr. S. Toliautas, Prof. J. Šulskus
Institute of Chemical Physics, Faculty of Physics
Vilnius University, Saulėtekio av. 9-III, 10222 Vilnius (Lithuania)

[c] Dr. J. Dodonova, Prof. S. Tumkevičius
Institute of Chemistry, Faculty of Chemistry and Geosciences
Vilnius University, Naugarduko str. 24, 03225 Vilnius (Lithuania)

[**] BODIPY = boron-dipyrromethene.

Supporting Information and the ORCID identification number(s) for the author(s) of this article can be found under: https://doi.org/10.1002/chem.201901315.

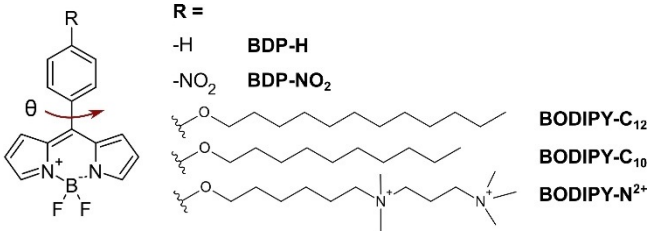

Figure 1. The molecular structures of the BODIPY-based molecular rotors examined in this work (**BDP-H** and **BDP-NO_2**) together with the widely used rotor BODIPY-C_{12} and its variants. The red arrow denotes intramolecular rotation, giving rise to viscosity-sensitivity of the fluorophores.

© 2019 Wiley-VCH Verlag GmbH & Co. KGaA, Weinheim

used molecular rotors.[6,8–10,14,25–29] These rotors have similar photophysical properties, and their main advantage is mono-exponential fluorescence decay, which simplifies data analysis and interpretation.[30] However, these molecules also have significant drawbacks. The first one is a short wavelength of fluorescence (≈515 nm). It is far shorter than preferred for experiments in thicker biological samples (>650 nm), where light scattering is an issue. The second disadvantage is the molecule's viscosity sensitivity, which drastically decreases above 1200 cP[10]—a significant disadvantage, which previously limited a study on the viscosity increase of aerosol particles under oxidation.[8] The last disadvantage is a dependence on solvent polarity and temperature,[31] which might lead to measuring erroneous values of viscosity in complex samples such as a living cell.

Solving the problems mentioned above requires a detailed understanding of the photophysical processes of BODIPY molecular rotors and how viscosity, temperature, and solvent polarity impact these processes. Previous theoretical work on **BDP-H** (Figure 1), which is very similar to BODIPY molecular rotors in structure, suggested that a partial charge transfer occurs when the fluorophore leaves the fluorescent state via the intramolecular rotation.[32] A different substituent on the phenyl ring should tune the ability of the ring to accept a charge. Therefore, we have examined **BDP-H** together with **BDP-NO$_2$** (Figure 1), which possesses a strong electron-withdrawing $-NO_2$ group, and contrasted the properties of both molecules with the ones of the BODIPY-C_{12} family of molecular rotors (Figure 1), which all contain mildly electron-donating -OR groups. Previously, **BDP-H** was explored as an accessory pigment for artificial molecular light harvesting systems,[33] whereas only basic spectroscopic properties (absorption and fluorescence spectra) of **BDP-NO$_2$** were examined.[34] However, the photophysical properties of these fluorophores were explored only in low viscosity solvents, which make their viscosity-sensitive properties completely unknown. Our goal was to examine how the substituent on the phenyl ring impacts the fluorophore's sensitivity to solvent polarity and ease the intramolecular rotation, which may tune the viscosity-sensitive properties of the molecule. Furthermore, by contrasting **BDP-H**, **BDP-NO$_2$**, and the family of BODIPY-C_{12} rotors, we sought to determine the viscosity-sensitive mechanism of BODIPY molecular rotors to a much greater depth than currently known, which is necessary for selective tuning of their properties.

Results and Discussion

The absorption spectra of both dyes consist of the main absorption band, which is located at 450–530 nm, and a higher energy band at 300–400 nm (Figure 2). The position of the main band did not significantly vary with the solvent for both dyes (Table 1). Additionally, a nitro group in **BDP-NO$_2$** did not seem to have a significant impact on the position of the absorption bands; the increasing electron-withdrawing capabilities of the $-NO_2$ group shifted the peak of absorption only by approximately 8 nm towards the red part of the visible spectrum. The substituent had a more significant effect on the fluorescence spectra. For **BDP-H**, the fluorescence band was located at 500–550 nm (Figure 2), producing a Stokes shift of 724 cm^{-1} (in toluene). Replacing $-H$ with the $-NO_2$ group increased the fluorescence wavelength by approximately 25 nm, resulting in an increase of Stokes shift to 1320 cm^{-1} (toluene). However, the position of the fluorescence bands for both **BDP-H** and **BDP-NO$_2$** did not strongly depend on the solvent (Table 1).

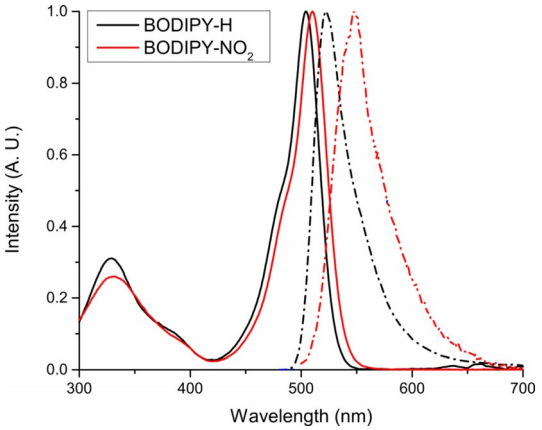

Figure 2. Absorption (solid) and fluorescence (dashed) spectra of **BDP-H** and **BDP-NO$_2$** in toluene. The absorption maxima are located at similar wavelengths, although the fluorescence spectrum of **BDP-NO$_2$** is more redshifted compared with **BDP-H**.

Table 1. Maxima of absorption (λ_{abs}^{max}) and emission (λ_F^{max}) spectra, fluorescence quantum yields (ϕ_F), and fluorescence lifetimes (τ_F) of **BDP-H** and **BDP-NO$_2$** in different solvents.

BDP-H	λ_{abs}^{max} [nm]	λ_F^{max} [nm]	ϕ_F [%]	τ_F [ps]
methanol	497	515	1.7	166
toluene	503	522	6.1	418
glycerol	502	518	69	4350
Castor oil	503	519	28	2220
BDP-NO$_2$				
methanol	505	541	0.23	23
toluene	511	548	0.68	65
glycerol	511	537	13	1143
Castor oil	511	538	13	1294

Both **BDP-H** and **BDP-NO$_2$** had higher fluorescence quantum yields and longer fluorescence lifetimes in viscous solvents (glycerol and Castor oil, Table 1), indicating that these fluorophores are sensitive to viscosity. Interestingly, **BDP-NO$_2$** had by far lower fluorescence quantum yields and fluorescence lifetimes than **BDP-H** in all solvents.

To investigate the viscosity-sensitivity of **BDP-H** and **BDP-NO$_2$** further as well as their sensitivity to solvent polarity, we have measured their fluorescence lifetime in a set of moderately polar methanol/glycerol mixtures and non-polar toluene/Castor oil mixtures at different temperatures (Figure 3). The absolute majority of fluorescence decays in methanol/glycerol mixtures were monoexponential, whereas the decays in toluene/Castor oil mixtures were biexponential owing to the contribution from Castor oil, which is itself fluorescent. In such

© 2019 Wiley-VCH Verlag GmbH & Co. KGaA, Weinheim

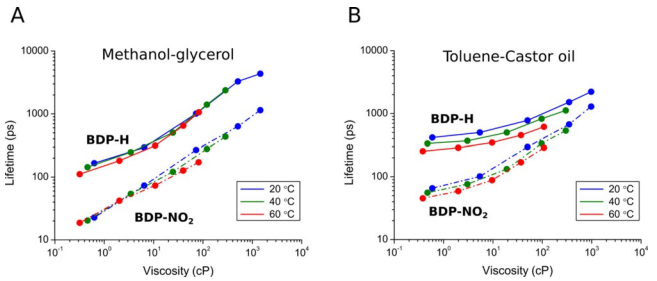

Figure 3. Fluorescence lifetimes of **BDP-H** (solid lines) and **BDP-NO$_2$** (dash-dotted lines) in moderately polar methanol/glycerol (A) and non-polar toluene/Castor oil (B) mixtures of varying viscosities and temperatures.

cases, intensity-weighted mean lifetimes are shown (Figure 3) unless the amplitude of the second component is below 10%, in which case only the lifetime of the dominant component is shown. More details together with the individual lifetimes and amplitudes are given in Figure S1 (in the Supporting Information). Four observations can be made from the data shown in Figure 3. The first one is that both dyes demonstrate an increase of fluorescence lifetime with viscosity at all conditions. Therefore, they are indeed molecular rotors. The second observation is that the lifetime–viscosity dependence in methanol/glycerol mixtures does not match the dependence in toluene/Castor oil at any temperature. Therefore, both dyes are somewhat sensitive to the polarity of the mixtures or their ability to form hydrogen bonds. This was previously observed with other BODIPY molecular rotors.[31] Thirdly, lifetime–viscosity dependencies measured at different temperatures do not overlap. From this, it follows that both **BDP-H** and **BDP-NO$_2$** have temperature dependence, that is, the temperature change affects the fluorescence lifetime not only by changing the solvent viscosity but by directly influencing the dyes. For example, in a hot solvent mixture, these dyes would have a slightly lower lifetime than in a colder solvent mixture of the same viscosity. Such behavior could arise from the presence of the activation energy barrier for intramolecular rotation, which was previously suggested for structurally similar BODIPY dyes.[31]

The final observation is that under all conditions **BDP-NO$_2$** has lower lifetimes than **BDP-H**. As the extinction coefficients ($\approx$50 000 $M^{-1}cm^{-1}$) are similar for both molecules, the radiative decay constants should not be drastically different. Therefore, the lower lifetimes of **BDP-NO$_2$** are likely to be a result of a faster non-radiative decay. This was confirmed by measuring the fluorescence lifetime of both dyes in poly(methyl methacrylate) (PMMA) and polystyrene polymer films. In a rigid polymer environment, non-radiative relaxation through intramolecular rotation should be almost entirely inhibited, and, therefore, the lifetime should mostly depend on the radiative relaxation rate. The intensity-weighted mean lifetimes of **BDP-H** in PMMA and polystyrene were 5850 ps and 5480 ps, respectively. The lifetimes of **BDP-NO$_2$** were not much different: 6280 ps in PMMA and 5500 ps in polystyrene. Therefore, both dyes have comparable fluorescence lifetimes in a rigid polymer matrix, which suggests that the lower fluorescence lifetime of **BDP-NO$_2$** in solvent mixtures is a result of a faster non-radiative deactivation of **BDP-NO$_2$** compared with **BDP-H** at the same viscosities. As a result, the fluorescence lifetime of **BDP-NO$_2$** should reach its maximum value at a much higher viscosity than the lifetime of **BDP-H**. This creates expectations that **BDP-NO$_2$** might be more useful for sensing viscosity in more rigid environments than **BDP-H** or other BODIPY molecular rotors (Figure 1).

Therefore, we set out to test both **BDP-H** and **BDP-NO$_2$** at viscosities well beyond 1000 cP. Such values can be reached in cooled glycerol, where viscosity rapidly increases with decreasing temperature down to the glass transition temperature of glycerol (190 K). The fluorescence decays of **BDP-NO$_2$** and **BDP-H** in cooled glycerol at various temperatures are shown in Figure 4. From the data shown in Figure 4A, it can be seen

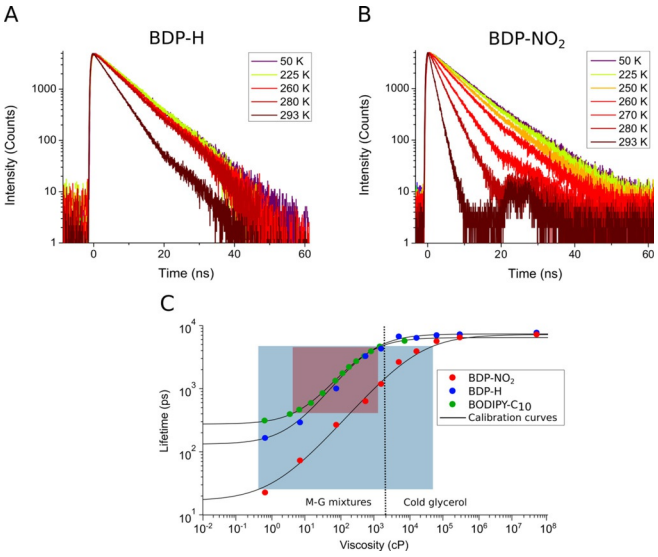

Figure 4. Time-resolved fluorescence decays of **BDP-H** (A) and **BDP-NO$_2$** (B) in cooled glycerol at temperatures from 293 K to 50 K. The glass transition temperature of glycerol is 190 K. C) Fluorescence lifetime-viscosity dependence of **BDP-H** (blue), **BDP-NO$_2$** (red), and BODIPY-C_{10} (green). The calibration curves were obtained by fitting the shown data points with the theoretically expected viscosity-lifetime dependence [Eq. (1)]. The rectangles denote lifetime dynamic ranges and viscosity-sensitive ranges for **BDP-NO$_2$** (cyan) and BODIPY-C_{10} (cherry red). The lifetimes measured in cooled glycerol (right side of the dotted line) are also affected by temperature, but this contribution is not significant (see main text).

that **BDP-H** reaches its maximum lifetime in glycerol at 280 K, where the viscosity is almost 5000 cP. Further reduction of temperature and the resulting increase in viscosity did not have any significant effect on the fluorescence decay of **BDP-H**. In contrast, the fluorescence decay of **BDP-NO$_2$** becomes progressively longer at temperatures down to 250 K, where the viscosity of glycerol becomes around 280 000 cP. Therefore, **BDP-NO$_2$** remains viscosity-sensitive at much larger viscosities compared with **BDP-H**. Additionally, the fluorescence decays of **BDP-NO$_2$** were monoexponential, which simplifies data analysis and dramatically reduces the photon counts required for viscosity assessment. The full set of lifetimes measured in solvent mixtures, cooled glycerol, and polymers is shown in Figure S2 (in the Supporting Information).

© 2019 Wiley-VCH Verlag GmbH & Co. KGaA, Weinheim

To fully contrast the viscosity-sensitivity ranges of **BDP-NO$_2$** and **BDP-H**, the lifetime–viscosity data at room temperature in methanol/glycerol mixtures and cooled glycerol is shown together with the previously reported data of BODIPY-C$_{10}$ in methanol/glycerol mixtures[31] in Figure 4C. BODIPY-C$_{10}$ is one of the BODIPY molecular rotors whose applications were reported in the literature previously (Figure 1), all of which have similar photophysical properties. The results in Figure 4C demonstrate that the viscosity-sensitive range of the **BDP-NO$_2$** surpasses the range of **BDP-H** and looks even more impressive compared with one of the most applied molecular rotors, BODIPY-C$_{10}$. The viscosity-sensitive range of the latter spans approximately 5 cP to 1500 cP, whereas **BDP-NO$_2$** is useful from 0.5 cP to 50 000 cP. As the lifetime below 200 ps might be difficult to resolve by using a conventional fluorescence lifetime imaging microscopy (FLIM) setup, performing viscosity measurements at viscosities below 50 cP might be challenging with **BDP-NO$_2$**. However, the strength of **BDP-NO$_2$** lies in its sensitivity at the 1000–50 000 cP range. This makes **BDP-NO$_2$** more applicable, especially when highly viscous samples are considered, such as semi-solid aerosols or cryogenically preserved tissues.

Such a wide viscosity-sensitive range of **BDP-NO$_2$** is not usual for BODIPY molecular rotors, and the reasons for it are far from obvious. Therefore, we have determined the action mechanism of the molecule and then have used it to explain the reasons behind this range of viscosity-sensitivity. To achieve this, we have globally analyzed fluorescence lifetime data, carried out femtosecond transient absorption experiments, and performed quantum chemical calculations.

It has been previously postulated that the temperature sensitivity of molecular rotors (Figure 3) may be caused by an energy barrier preventing rapid intramolecular rotation and relaxation from the fluorescent state.[31] Therefore, we set out to find out the height of the barrier for **BDP-H** and **BDP-NO$_2$**. This has been achieved by fitting the lifetime dataset with the previously derived fluorescence lifetime dependence on viscosity and temperature [Eq. (1)]:[31]

$$\tau = \frac{1}{\frac{1}{C\eta^x + {}^1/_{k_{nr,\max}}} e^{-E_a/kT} + k_f} \qquad (1)$$

where τ is the fluorescence lifetime, η is the viscosity, T is the temperature, x is a constant showing the degree of fluorescence lifetime sensitivity to viscosity, E_a is the activation energy barrier, $k_{nr,max}$ is the maximum achievable non-radiative decay constant at infinite temperature and zero viscosity (which is also an inverse of the lowest possible fluorescence lifetime), k is the Boltzmann's constant, k_f is the rate constant of fluorescence, and C is a constant that determines the minimum viscosity at which the fluorophore is still viscosity-sensitive. Equation (1) was derived by using the Förster–Hoffmann equation[35] as a starting point, which correctly describes the fluorescence lifetime-viscosity dependence of molecular rotors at intermediate viscosities.[2] Additional terms were added to account for the fluorescence lifetime independence of viscosity at the very low and very high viscosity limits and the result was combined with the Arrhenius equation, which accounts for the temperature-dependence. Equation (1) successfully fitted the fluorescence lifetime dependence on viscosity and temperature of a few other BODIPY molecular rotors,[31] but its theoretical basis has not been validated by theoretical calculations.

The global fits of the fluorescence lifetime datasets of **BDP-H** and **BDP-NO$_2$** obtained by using Equation (1) are shown in Figure S3 (in the Supporting Information) and the fitting parameters are in Table S1 (in the Supporting Information). The critical parameters extracted from the fits are shown in Table 2.

Table 2. Parameters determining the viscosity- and temperature-sensitivity of **BDP-NO$_2$** and **BDP-H** calculated from the fitting parameters (Table S1 in the Supporting Information) of the global fits shown in Figure S3 (in the Supporting Information) obtained by using Equation (1).

Solvent mixture	Molecular rotor	x	E_a [meV]
toluene/Castor oil	**BDP-H**	0.56	103
	BDP-NO$_2$	0.65	72
methanol/glycerol	**BDP-H**	0.76	32
	BDP-NO$_2$	0.58	52

The constant x (Table 1), which denotes viscosity sensitivity, is similar for both molecules. Although the energy barriers in methanol/glycerol are low and difficult to determine accurately from the fit, **BDP-NO$_2$** has a lower energy barrier preventing intramolecular rotation in toluene/Castor oil mixtures. The lower energy barrier should lead to a faster non-radiative relaxation and a shorter fluorescence lifetime of **BDP-NO$_2$** at the same viscosity conditions. This should also result in a more extended viscosity-sensitive range of **BDP-NO$_2$** because higher viscosity would be required to suppress non-radiative relaxation. The knowledge of the fitting parameters has allowed us to subsequently calculate how much the temperature contributes to the change in fluorescence lifetimes in cold glycerol, which are shown in Figure 4C. We have calculated the lifetimes the dyes are expected to have at viscosities equal to the ones in cooled glycerol but at room temperature. This led to a minor reduction in lifetimes compared with the measured ones in cold glycerol; the details are given in Figure S4 (in the Supporting Information).

To determine what happens to BODIPY molecular rotors after they leave the fluorescent state, we have performed ultrafast transient absorption experiments. Previous studies of **BDP-H**[36] revealed that **BDP-H** does not enter any long-lived intermediate states upon leaving the fluorescent state and returns to the ground state either via a conical intersection or a very fast internal conversion. In the light of these previously obtained results, we have tested if **BDP-NO$_2$** follows a similar mechanism upon excitation. The obtained transient absorption spectra in toluene are shown in Figure 5. The detailed explanations are provided in the Supporting Information. As the spectrum is no longer visible at the pump-probe delay of 1000 ps, this demonstrates that **BDP-NO$_2$** does not enter any long-lived state either. Additionally, the dominant exponential compo-

© 2019 Wiley-VCH Verlag GmbH & Co. KGaA, Weinheim

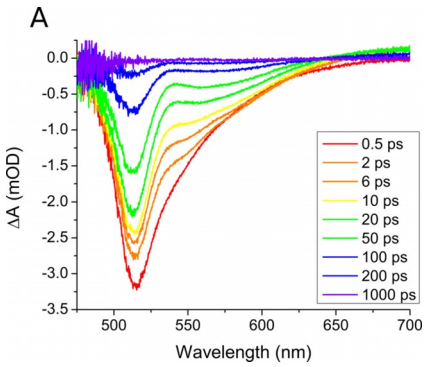

Figure 5. Transient absorption spectra of **BDP-NO$_2$** in toluene. The spectra consist of closely overlapping ground state bleach (GSB) and stimulated emission (SE) bands.

nent in the ground state bleach signal of **BDP-NO$_2$** has a lifetime of 81 ps (Figure S6 in the Supporting Information). The fact that it is close to the fluorescence lifetime of **BDP-NO$_2$** in toluene (65 ps) means that the molecule returns to the ground state almost immediately after leaving the fluorescent state. Therefore, the transient absorption spectra do not show any evidence of any other state besides the ground and the fluorescent states.

To complement our results from femtosecond transient absorption experiments and from global fits of fluorescence lifetime data, we have performed quantum chemical calculations that determined the energy of the ground (S_0) and first excited (S_1) electronic states of the studied compounds with respect to the dihedral angle Θ between the phenyl group and the BODIPY core. Excited-state optimizations were used to determine the relaxed surface of the S_1 state and the corresponding energy of the S_0 state. The effects of the solvent environment were included by using the continuum model. Toluene was used as the model solvent as the possible hydrogen bonding between the dye and solvent molecules complicate the task of equivalent modeling of methanol or glycerol.

The comparison of theoretically predicted excitation and emission energies with experimental ones is shown in Table S2 (in the Supporting Information). The cross-sections of potential energy surfaces (PES) using the dihedral angle Θ as the reaction coordinate for **BDP-H** and **BDP-NO$_2$** are shown in Figure 6A. The curves of the first excited electronic state (S_1) of both compounds are contrasted in Figure 6B, where the energy of the local minimum at approximately 45° is set to 0 eV as a reference point. Molecular geometries at various points on the PES, together with the dihedral angle Θ and an out-of-plane bend of the BODIPY core ω, are shown in Figure 6C. Ground state minima of the fluorophores are located at the dihedral angle value of about 53°, which is very close to the angle previously obtained from crystallographic data and theoretical calculations of **BDP-H**.[33,36] The shapes of the curves on the calculated PES suggest the following reaction mechanism: when excited, the fluorophores rapidly relax from the higher vibrational levels to the nearby local minimum ($S_{1,m}$) from where the fluorescence takes place. However, because of the thermal energy available, the fluorophores can cross the

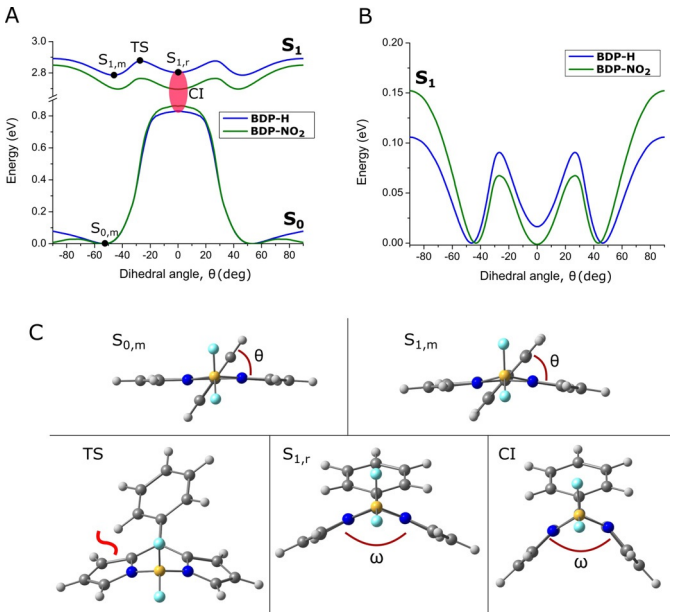

Figure 6. A) Potential energy surface (PES) cross-sections of the ground and lowest excited electronic states for **BDP-H** (blue) and **BDP-NO$_2$** (green) corresponding to the single reaction coordinate on the excited-state surface—the change of the dihedral angle θ between the BODIPY core and the phenyl group. B) Comparison of the PES of the first excited electronic state. The energy of the local minimum at approximately 45° is set to 0 eV as a reference point for easier comparison. C) Molecular structures of **BDP-H** at the points of interest on the PES: ground-state minimum $S_{0,m}$, excited-state minima $S_{1,m}$ and $S_{1,r}$ a transition state between the two S_1 minima (TS), and the vicinity of the intersection between ground and excited states near $S_{1,r}$ (CI). The geometries of **BDP-NO$_2$** are almost identical to the ones shown. The dihedral angle θ and out-of-plane bend angle ω are also marked. All geometries are shown from the same viewpoint except for the TS geometry, which is slightly tilted to reveal the steric repulsion between H atoms giving rise to the energy barrier TS (highlighted by a red curve).

approximately 0.1 eV barrier, located at around 27°, and reach another minimum ($S_{1,r}$) at 0° on the PES of the excited state. As the transient absorption data demonstrate that the fluorophores relax rapidly to the ground state after leaving the fluorescent state, it means that a non-radiative pathway to the ground state (possibly a conical intersection) is likely to exist in the vicinity of the $S_{1,r}$ structure. This has also been suggested previously for **BDP-H** and other similar molecules.[32,37] According to our calculations, an increase in the out-of-plane bend (ω) of the BODIPY core close to $S_{1,r}$ indeed results in a geometry (Figure 6C, labeled CI) where ground- and excited-state energies start rapidly approaching each other, indicating the presence of the crossing point (for more details, see Figure S7 in the Supporting Information). Afterwards, the molecule relaxes in the ground state, returning to the minimum $S_{0,m}$.

One of the main findings of the theoretical calculations is the presence of the small, but not vanishing, energy barrier (Figure 6A, B at 27° angle) replicating the energy values obtained from fitting the lifetime dataset. The calculated S_1 energy curves result in barriers of 91 and 67 meV for **BDP-H** and **BDP-NO$_2$**, respectively, which are caused by repulsion between two H atoms, as shown in Figure 6C (TS, red line). In comparison, the values obtained from the lifetime fits in toluene/Castor oil mixtures at varying temperatures are 103 and

© 2019 Wiley-VCH Verlag GmbH & Co. KGaA, Weinheim

72 meV (Table 2). The close agreement validates both our theoretical calculations and the rationale behind the derivation of Equation (1).[31] These results provide strong evidence that the temperature dependence of BODIPY molecular rotors is indeed caused by the presence of an energy barrier preventing the non-radiative relaxation from the fluorescent state.

Figure 6B compares the PES of the fluorophores in the excited state and reveals critical differences between **BDP-H** and **BDP-NO$_2$**. The most important observation is that the presence of the $-NO_2$ group stabilizes the S_1 state of the fluorophore when the dihedral angle is close to 0°. This is a result of the shape of the LUMO (Figure S8 in the Supporting Information). Owing to the electron-withdrawing abilities of the $-NO_2$ group, the electron density becomes greater on the phenyl ring and on the bond connecting the ring to the BODIPY core. Therefore, the LUMO becomes stabilized to a greater degree when the dihedral angle is low owing to a better overlap of p orbitals, as indicated by the decrease of the calculated energy level of the LUMO (Table S3 in the Supporting Information). In contrast, for both molecules, the HOMO has a nodal plane (Figure S8 in the Supporting Information) along the central axis of the molecule and its energy is barely sensitive to the dihedral angle. As a result, when the fluorophore is excited, and the LUMO is populated, the molecule becomes able to planarize, and the process is more favorable when the $-NO_2$ group is present.

Greater stabilization at 0° dihedral angle for **BDP-NO$_2$** causes two effects: the energy barrier is reduced and the $S_{1,m}$ minimum gets shifted closer to 0° by approximately 3 degrees. The reduction of the barrier by approximately 30 meV should make the non-radiative relaxation rate faster by a factor of 3 at room temperature, as predicted by Equation (1). Given that the fluorescence lifetimes of **BDP-NO$_2$** are shorter approximately by a factor of 2 to 6 depending on the environment, an additional increase of the non-radiative relaxation rate of **BDP-NO$_2$** might be a result of a smaller dihedral angle in $S_{1,m}$ geometry. As a result, a smaller structural change is required for the molecule to reach the top of the energy barrier from $S_{1,m}$. A lower degree of movement during the relaxation would then result in less hindrance by the viscous environment. This is supported by the calculation results: the cumulative sum of the change in atomic coordinates between $S_{1,m}$ and TS structures is lower by approximately 20% for **BDP-NO$_2$** (Figure S9 in the Supporting Information). This could be an additional factor that makes intramolecular rotation quicker, fluorescence lifetime lower, and the viscosity-sensitive range wider for **BDP-NO$_2$**.

Conclusions

We have shown that by introducing a $-NO_2$ group into the structure of a BODIPY molecular rotor we have managed to improve its viscosity-sensing properties drastically. The resulting viscosity-sensitive range (0.5–50000 cP) is larger by over two orders of magnitude, which makes it, to our knowledge, the only hydrophobic molecular rotor suitable for viscosity measurements in high viscosity environments. Although performing measurements in non-viscous samples might be challenging with **BDP-NO$_2$** owing to its low lifetime at <50 cP viscosities, this region can be covered by using previously reported BODIPY molecular rotors such as BODIPY-C_{10} or BODIPY-C_{12}. In addition, with the help of quantum chemical calculations, we have determined the photophysical mechanism of BODIPY rotors, which was known in much less detail. Our determined mechanism demonstrates that the viscosity-sensitive range of **BDP-NO$_2$** is widened because the electron-withdrawing $-NO_2$ group makes the intramolecular rotation of the fluorophore in the excited state less impeded by an energy barrier to rotation, which then preserves the viscosity-sensitivity of the probe even in high viscosity environments. It is likely that a similar result could be achieved by introducing other electron-withdrawing substituents besides the $-NO_2$ group. Our results also show that the temperature-sensitivity of BODIPY molecular rotors is indeed caused by the presence of an energy barrier to intramolecular rotation. Besides reporting a new molecular rotor with attractive properties, this study also provides a deeper insight into how molecular rotors work, why they could be sensitive both to viscosity and temperature, and how their properties could be purposefully tuned, thus avoiding empirical screening of a library of fluorophores for desired properties.

Experimental Section

Dyes, reagents, and solvents

Stock solutions of fluorophores were made in toluene (2–5 mM concentrations) and diluted for further experiments in solvents or their mixtures of interest. Methanol and glycerol were obtained from Sigma–Aldrich. Toluene was obtained from Riedel-de-Haen. Castor oil was obtained from Sigma. The molar masses of PMMA (Aldrich) and polystyrene (Fluka) were 350000 g mol^{-1} and 200000 g mol^{-1}, respectively. The viscosities of methanol/glycerol and toluene/Castor oil mixtures were measured by using a Stabinger viscometer (SVM3000, Anton Paar). Polymer films were made by first dissolving polymer (2 mg mL^{-1}) and a BODIPY fluorophore (2.5 μg mL^{-1}) in chloroform and then by spin-coating the solution on a glass slide.

Reagents and solvents for the organic synthesis of **BDP-H** and **BDP-NO$_2$** were purchased directly from commercial suppliers; solvents were purified by known procedures. Thin layer chromatography was performed by using TLC aluminum sheets with silica gel (Merck 60 F254). Visualization was accomplished by UV light. Column chromatography was performed by using silica gel 60 (0.040–0.063 mm; Merck). NMR spectra were recorded with a Bruker Ascend 400 (400 MHz for ^{1}H, 128.4 MHz for ^{11}B, 376.5 MHz for ^{19}F). NMR spectra were referenced to residual solvent peaks. Melting points were determined in open capillaries with a digital melting point IA9100 series apparatus (Thermo Fischer Scientific) and were not corrected. More details on the organic synthesis and the NMR spectra of products are shown in the Supporting Information.

Absorption, steady-state, and time-resolved fluorescence

Absorption spectra were measured by using a Jasco V-670 spectrophotometer. Fluorescence spectra were recorded with an Edin-

© 2019 Wiley-VCH Verlag GmbH & Co. KGaA, Weinheim

burgh-F900 (Edinburgh Instruments) fluorometer. A picosecond pulsed diode laser EPL-470 (Edinburgh Instruments) emitting approximately 100 ps pulses at 473 nm (2 MHz frequency) was used as an excitation source. Quartz cuvettes (10 mm) were used for both absorption and fluorescence measurements. The fluorophores' concentrations were up to 5 μM. The fluorescence decays at 23 °C, 40 °C, and 60 °C and in cold glycerol were measured by using two setups. The first one consists of a C5680 streak camera (Hamamatsu) in photon counting mode. The fluorescence signal was dispersed by using an Acton SP2150 monochromator (Princeton Instruments). The excitation source was composed of a femtosecond Yb:KGW oscillator (Light Conversion Ltd.), producing 80 fs pulses at 1030 nm, 76 MHz. The laser radiation was frequency-tripled to 343 nm by using a HIRO harmonics generator (Light Conversion). Fluorescence decays with lifetimes below approximately 500 ps were recorded with a streak camera using a M5675 synchroscan sweep unit (time resolution up to 3 ps). The longer decays were recorded by using a M5677 slow single-sweep unit. Fluorescence decays had 1000 to 10000 counts at the peak of the decay. The temperature was controlled with a home-built system employing an aluminum cuvette casing with a Peltier element. Quartz cuvettes with 2 mm path length were used. The second setup consisted of the aforementioned Edinburgh-F900 (Edinburgh Instruments) fluorometer using the same excitation source (EPL-470 diode laser). The measurement method for fluorescence decays was time-correlated single photon counting (TCSPC). A time window of 100 ns was used with 4096 channels. The time resolution of the setup was approximately 250 ps. Heating was done by using an Alpha RA 8 cooling thermostat (LAUDA). Cooling was achieved by using a closed-cycle liquid helium cold finger cryostat (Janis CCS-100/204). The viscosities of cooled glycerol were calculated by using the empirical formula suggested by Schroeter et al.[38]

Femtosecond transient absorption

The femtosecond transient absorption setup was based on a Pharos 10–600-PP laser (Light Conversion Ltd.) lasing at 1028 nm with a 200 kHz frequency and producing 290 fs pulses. For experiments, the frequency was reduced to 4.76 kHz. The laser wavelength was varied by using Orpheus PO15F2L collinear optical parametric amplifier (Light Conversion Ltd.). The laser beam was separated into "pump" and "probe" beams. The pumping wavelength for the experiment was set to 470 nm, whereas the "probe" beam was sent through a Ti:sapphire crystal to generate a continuum spanning the 475–800 nm range. The polarization of the "pump" beam was set to the magic angle with respect to the polarization of the "probe" beam. The transient absorption signal was detected by using an Andor-Shamrock SR-500i-B1-R spectrometer (Andor Technology) with Andor–Newton (Andor Technology) DU970 CCD camera (1600×200 pixels), and a diffraction grating (150 lines mm^{-1}).

Data analysis

Fluorescence decays were fitted by using home-written codes in MATLAB R2012a (MathWorks) and Labview 16.0 (National Instruments). For multiexponential decays, intensity-weighted mean lifetimes were calculated [Eq. (2)]:

$$\bar{\tau} = \frac{\sum_i a_i \tau_i^2}{\sum_i a_i \tau_i} \qquad (2)$$

Further data processing and analysis was done with OriginPro 8.6.

Theoretical calculations

All calculations are performed using the electronic structure modeling package Gaussian09[39] at the level of density functional theory (DFT),[40] as well as time-dependent DFT[41] for the excited-state properties. After preliminary study, a combination of M06-2X functional[42] and cc-pVDZ basis set[43] was chosen for the subsequent computations; use of M06-2X for the calculation of the optical properties of BODIPY-based dimers has been previously validated by functional benchmarks.[44] Bulk solvent effects on the investigated compounds were modeled by using the conductor-like polarizable continuum model (C-PCM)[45] with solvent parameters of toluene. Additional analysis and visualization of the calculated molecular structures were done with the ChemCraft graphical program.[46]

Acknowledgments

This research was funded by a grant (No. S-MIP-19-6) from the Research Council of Lithuania. Quantum chemical computations were carried out by using resources at the High-Performance Computing Center "HPC Sauletekis" (Vilnius University, Faculty of Physics). We also thank Prof. Vidmantas Gulbinas for advice on writing the manuscript.

Conflict of interest

The authors declare no conflict of interest.

Keywords: fluorescence spectroscopy · molecular rotors · time-dependent density functional theory (TD-DFT) · viscosity sensing

[1] M. A. Haidekker, M. Nipper, A. Mustafic, D. Lichlyter, M. Dakanali, E. A. Theodorakis, *Dyes with Segmental Mobility: Molecular Rotors*, Springer, Berlin, **2010**.
[2] M. K. Kuimova, *Phys. Chem. Chem. Phys.* **2012**, *14*, 12671 – 12686.
[3] J. M. Nölle, C. Jüngst, A. Zumbusch, D. Wöll, *Polym. Chem.* **2014**, *5*, 2700 – 2703.
[4] H. Doan, S. L. Raut, D. Yale, M. Balaz, S. V. Dzyuba, Z. Gryczynski, *Chem. Commun.* **2016**, *52*, 9510 – 9513.
[5] N. P. Kamat, Z. Z. Liao, L. E. Moses, J. Rawson, M. J. Therien, I. J. Dmochowski, D. A. Hammer, *Proc. Natl. Acad. Sci. USA* **2011**, *108*, 13984 – 13989.
[6] N. A. Hosny, C. Fitzgerald, C. Tong, M. Kalberer, M. K. Kuimova, F. D. Pope, *Faraday Discuss.* **2013**, *165*, 343 – 356.
[7] N. A. Hosny, C. Fitzgerald, A. Vyšniauskas, T. Athanasiadis, T. Berkemeier, N. Uygur, U. Pöschl, M. Shiraiwa, M. Kalberer, F. D. Pope, M. K. Kuimova, *Chem. Sci.* **2016**, *7*, 1357 – 1367.
[8] T. Athanasiadis, C. Fitzgerald, N. Davidson, C. Giorio, S. W. Botchway, A. D. Ward, M. Kalberer, F. D. Pope, M. K. Kuimova, *Phys. Chem. Chem. Phys.* **2016**, *18*, 30385 – 30393.
[9] A. Vyšniauskas, M. Qurashi, M. K. Kuimova, *Chem. Eur. J.* **2016**, *22*, 13210 – 13217.
[10] M. R. Dent, I. Lopez Duarte, C. J. Dickson, N. D. Geoghegan, J. M. Cooper, I. R. Gould, R. Krams, J. A. Bull, N. J. Brooks, M. K. Kuimova, *Phys. Chem. Chem. Phys.* **2015**, *17*, 18393 – 18402.
[11] A. J. Thompson, T. W. Herling, M. Kubankova, A. Vyšniauskas, T. P. J. Knowles, M. K. Kuimova, *J. Phys. Chem. B* **2015**, *119*, 10170 – 10179.
[12] X. J. Peng, Z. G. Yang, J. Y. Wang, J. L. Fan, Y. X. He, F. L. Song, B. S. Wang, S. G. Sun, J. L. Qu, J. Qi, M. Yang, *J. Am. Chem. Soc.* **2011**, *133*, 6626 – 6635.

© 2019 Wiley-VCH Verlag GmbH & Co. KGaA, Weinheim

[13] E. Gatzogiannis, Z. Chen, L. Wei, R. Wombacher, Y.-T. Kao, G. Yefremov, V. W. Cornish, W. Min, *Chem. Commun.* **2012**, *48*, 8694 – 8696.
[14] M. K. Kuimova, G. Yahioglu, J. A. Levitt, K. Suhling, *J. Am. Chem. Soc.* **2008**, *130*, 6672 – 6673.
[15] M. K. Kuimova, S. W. Botchway, A. W. Parker, M. Balaz, H. A. Collins, H. L. Anderson, K. Suhling, P. R. Ogilby, *Nat. Chem.* **2009**, *1*, 69 – 73.
[16] Z. Yang, Y. He, J.-H. Lee, N. Park, M. Suh, W.-S. Chae, J. Cao, X. Peng, H. Jung, C. Kang, J. S. Kim, *J. Am. Chem. Soc.* **2013**, *135*, 9181 – 9185.
[17] N. Jiang, J. Fan, S. Zhang, T. Wu, J. Wang, P. Gao, J. Qu, F. Zhou, X. Peng, *Sensors Actuators B Chem.* **2014**, *190*, 685 – 693.
[18] L. Wang, Y. Xiao, W. Tian, L. Deng, *J. Am. Chem. Soc.* **2013**, *135*, 2903 – 2906.
[19] Z. Yang, Y. He, J. H. Lee, W.-S. Chae, W. Ren, J. H. Lee, C. Kang, J. S. Kim, *Chem. Commun.* **2014**, *50*, 11672 – 11675.
[20] M. R. Dent, I. López-Duarte, C. J. Dickson, P. Chairatana, H. L. Anderson, I. R. Gould, D. Wylie, A. Vyšniauskas, N. J. Brooks, M. K. Kuimova, *Chem. Commun.* **2016**, *52*, 13269 – 13272.
[21] I. López-Duarte, T. T. Vu, M. A. Izquierdo, J. A. Bull, M. K. Kuimova, *Chem. Commun.* **2014**, *50*, 5282 – 5284.
[22] J. Korlach, P. Schwille, W. Webb, G. W. Feigenson, *Proc. Natl. Acad. Sci. USA* **1999**, *96*, 8461 – 8466.
[23] M. Edidin, Y. Zagyansky, T. J. Lardner, *Science* **2003**, *191*, 466 – 468.
[24] M. Dahan, S. Le, C. Luccardini, *Science* **2003**, *302*, 442 – 445.
[25] Y. Wu, M. Stefl, A. Olzyńska, M. Hof, G. Yahioglu, P. Yip, D. R. Casey, O. Ces, J. Humpolíčková, M. K. Kuimova, *Phys. Chem. Chem. Phys.* **2013**, *15*, 14986 – 14993.
[26] N. A. Hosny, G. Mohamedi, P. Rademeyer, J. Owen, Y. Wu, M.-X. Tang, R. J. Eckersley, E. Stride, M. K. Kuimova, *Proc. Natl. Acad. Sci. USA* **2013**, *110*, 9225 – 9230.
[27] T.-Y. Dora Tang, C. Rohaida Che Hak, A. J. Thompson, M. K. Kuimova, D. S. Williams, A. W. Perriman, S. Mann, *Nat. Chem.* **2014**, *6*, 527 – 533.
[28] J. E. Chambers, M. Kubánková, R. G. Huber, I. López-Duarte, E. Avezov, P. J. Bond, S. J. Marciniak, M. K. Kuimova, *ACS Nano* **2018**, *12*, 4398 – 4407.
[29] I. E. Steinmark, A. L. James, P. H. Chung, P. E. Morton, M. Parsons, C. A. Dreiss, C. D. Lorenz, G. Yahioglu, K. Suhling, *PLoS One* **2019**, *14*, e0211165.
[30] J. A. Levitt, P.-H. Chung, M. K. Kuimova, G. Yahioglu, Y. Wang, J. Qu, K. Suhling, *ChemPhysChem* **2011**, *12*, 662 – 672.
[31] A. Vyšniauskas, I. López-Duarte, N. Duchemin, T.-T. Vu, Y. Wu, E. M. Budynina, Y. A. Volkova, E. Peña Cabrera, D. E. Ramírez-Ornelas, M. K. Kuimova, *Phys. Chem. Chem. Phys.* **2017**, *19*, 25252 – 25259.
[32] A. Prlj, L. Vannay, C. Corminboeuf, *Helv. Chim. Acta* **2017**, *100*, e1700093.
[33] F. Li, S. I. Yang, Y. Ciringh, J. Seth, C. H. Martin, D. L. Singh, D. Kim, R. R. Birge, D. F. Bocian, D. Holten, J. S. Lindsey, *J. Am. Chem. Soc.* **1998**, *120*, 10001 – 10017.
[34] A. C. Benniston, S. Clift, A. Harriman, *J. Mol. Struct.* **2011**, *985*, 346 – 354.
[35] T. Forster, G. Hoffmann, *Zeitschr. Phys. Chem.* **1971**, *75*, 63 – 76.
[36] H. L. Kee, C. Kirmaiery, L. Yu, P. Thamyongkit, W. J. Youngblood, M. E. Calder, L. Ramos, B. C. Noll, D. F. Bocian, W. R. Scheldt, R. R. Birge, J. S. Lindsey, D. Holten, *J. Phys. Chem. B* **2005**, *109*, 20433 – 20443.
[37] T. Suhina, S. Amirjalayer, S. Woutersen, D. Bonn, A. M. Brouwer, *Phys. Chem. Chem. Phys.* **2017**, *19*, 19998 – 20007.
[38] K. Schröter, E. Donth, *J. Chem. Phys.* **2000**, *113*, 9101 – 9108.
[39] Gaussian 09, Revision D.01, M. J. Frisch, G. W. Trucks, H. B. Schlegel, G. E. Scuseria, M. A. Robb, J. R. Cheeseman, G. Scalmani, V. Barone, B. Mennucci, G. A. Petersson, H. Nakatsuji, M. Caricato, X. Li, H. P. Hratchian, A. F. Izmaylov, J. Bloino, G. Zheng, J. L. Sonnenberg, M. Hada, M. Ehara, K. Toyota, R. Fukuda, J. Hasegawa, M. Ishida, T. Nakajima, Y. Honda, O. Kitao, H. Nakai, T. Vreven, J. A. Montgomery, Jr., J. E. Peralta, F. Ogliaro, M. Bearpark, J. J. Heyd, E. Brothers, K. N. Kudin, V. N. Staroverov, R. Kobayashi, J. Normand, K. Raghavachari, A. Rendell, J. C. Burant, S. S. Iyengar, J. Tomasi, M. Cossi, N. Rega, J. M. Millam, M. Klene, J. E. Knox, J. B. Cross, V. Bakken, C. Adamo, J. Jaramillo, R. Gomperts, R. E. Stratmann, O. Yazyev, A. J. Austin, R. Cammi, C. Pomelli, J. W. Ochterski, R. L. Martin, K. Morokuma, V. G. Zakrzewski, G. A. Voth, P. Salvador, J. J. Dannenberg, S. Dapprich, A. D. Daniels, Ö. Farkas, J. B. Foresman, J. V. Ortiz, J. Cioslowski, D. J. Fox, Gaussian, Inc. Wallingford CT, **2013**.
[40] R. G. Parr, W. Yang, *Density-Functional Theory of Atoms and Molecules*, Oxford University Press, Oxford, **1989**.
[41] R. E. Stratmann, G. E. Scuseria, M. J. Frisch, *J. Chem. Phys.* **1998**, *109*, 8218.
[42] Y. Zhao, D. G. Truhlar, *Theor. Chem. Acc.* **2008**, *120*, 215 – 241.
[43] R. A. Kendall, T. H. Dunning, R. J. Harrison, *J. Chem. Phys.* **1992**, *96*, 6796 – 6806.
[44] M. R. Momeni, A. Brown, *J. Phys. Chem. A* **2016**, *120*, 2550 – 2560.
[45] M. Cossi, N. Rega, G. Scalmani, V. Barone, *J. Comput. Chem.* **2003**, *24*, 669 – 681.
[46] G. A. Andrienko, ChemCraft, v1.8, build 536, **2018**.

Manuscript received: March 21, 2019
Accepted manuscript online: April 18, 2019
Version of record online: June 27, 2019

© 2019 Wiley-VCH Verlag GmbH & Co. KGaA, Weinheim